Defense Threat Reduction Agency
8725 John J. Kingman Road, MS-6201
Fort Belvoir, VA 22060-6201

DTRA-TR-15-16

TECHNICAL REPORT

Development of Mouse Lung Deposition Models

July 2015

DTRA01-03-D-0014

Dr. Bahman Asgharian

Prepared by:
Applied Research Associates
8537 Six Forks Road
Suite 600
Raleigh, NC 27615

DESTRUCTION NOTICE:

Destroy this report when it is no longer needed.
Do not return to sender.

PLEASE NOTIFY THE DEFENSE THREAT REDUCTION AGENCY, ATTN: DTRIAC/ J9STT, 8725 JOHN J. KINGMAN ROAD, MS-6201, FT BELVOIR, VA 22060-6201, IF YOUR ADDRESS IS INCORRECT, IF YOU WISH THAT IT BE DELETED FROM THE DISTRIBUTION LIST, OR IF THE ADDRESSEE IS NO LONGER EMPLOYED BY YOUR ORGANIZATION.

REPORT DOCUMENTATION PAGE

Form Approved
OMB No. 0704-0188

1. REPORT DATE *(DD-MM-YYYY)*	**2. REPORT TYPE**	**3. DATES COVERED** *(From - To)*
00-07-2015	Technical	February 10, 2011 - October 7, 2012

4. TITLE AND SUBTITLE

Development of Mouse Lung Deposition Models

5a. CONTRACT NUMBER

DTRA01-03-D-0014-0030

5b. GRANT NUMBER

5c. PROGRAM ELEMENT NUMBER

6. AUTHOR(S)

Dr. Bahman Asgharian

5d. PROJECT NUMBER

5e. TASK NUMBER

5f. WORK UNIT NUMBER

7. PERFORMING ORGANIZATION NAME(S) AND ADDRESS(ES)

Applied Research Associates, Inc.
8537 Six Forks Rd.
Suite 600
Raleigh, NC 27615

8. PERFORMING ORGANIZATION REPORT NUMBER

9. SPONSORING / MONITORING AGENCY NAME(S) AND ADDRESS(ES)

Defense Threat Reduction Agency
8725 John J. Kingman Road, MS 6201
Fort Belvoir, VA 22060-6201

10. SPONSOR/MONITOR'S ACRONYM(S)

DTRA

11. SPONSOR/MONITOR'S REPORT NUMBER(S)

DTRA-TR-15-16

12. DISTRIBUTION / AVAILABILITY STATEMENT

Distribution Statement A. Approved for public release; distribution is unlimited.

13. SUPPLEMENTARY NOTES

14. ABSTRACT

Mathematical models were developed to predict deposition of inhaled particles in the lungs of two strains of mice. The deposition model included an algorithm to calculate particle inhalability. Model predictions included filtering capabilities in the nasal passages, and deposition in various regions of the lung. Particle inhalability was smallest in mice compared with that for larger rodents and humans. In addition, there was a significant deposition of particles in the nasal passages, with the consequence of limited penetration of particles into the lung. As a result, particle deposition in lung airways was small, particularly for larger particles. The findings from the study indicated that mice inhalation studies should be conducted with sub-micrometer particles to allow for sufficient deposition in the lung to produce the desired biological responses.

15. SUBJECT TERMS

Mouse Lung Geometry Lung Deposition Modeling Inhalability Regional Deposition

16. SECURITY CLASSIFICATION OF:			**17. LIMITATION OF ABSTRACT**	**18. NUMBER OF PAGES**	**19a. NAME OF RESPONSIBLE PERSON**
a. REPORT	**b. ABSTRACT**	**c. THIS PAGE**	SAR	28	Richard Fry
Unclassified	Unclassified	Unclassified			**19b. TELEPHONE NUMBER** *(include area code)* 703-767-3193

CONVERSION TABLE

Conversion Factors for U.S. Customary to metric (SI) units of measurement.

MULTIPLY →	BY →	TO GET
← TO GET	← BY	← DIVIDE
angstrom	1.000 000 x E -10	meters (m)
atmosphere (normal)	1.013 25 x E +2	kilo pascal (kPa)
bar	1.000 000 x E +2	kilo pascal (kPa)
barn	1.000 000 x E -28	meter^2 (m^2)
British thermal unit (thermochemical)	1.054 350 x E +3	joule (J)
calorie (thermochemical)	4.184 000	joule (J)
cal (thermochemical/cm^2)	4.184 000 x E -2	mega joule/m^2 (MJ/m^2)
curie	3.700 000 x E +1	*giga bacquerel (GBq)
degree (angle)	1.745 329 x E -2	radian (rad)
degree Fahrenheit	$t_k = (t^of + 459.67)/1.8$	degree kelvin (K)
electron volt	1.602 19 x E -19	joule (J)
erg	1.000 000 x E -7	joule (J)
erg/second	1.000 000 x E -7	watt (W)
foot	3.048 000 x E -1	meter (m)
foot-pound-force	1.355 818	joule (J)
gallon (U.S. liquid)	3.785 412 x E -3	meter^3 (m^3)
inch	2.540 000 x E -2	meter (m)
jerk	1.000 000 x E +9	joule (J)
joule/kilogram (J/kg) radiation dose absorbed	1.000 000	Gray (Gy)
kilotons	4.183	terajoules
kip (1000 lbf)	4.448 222 x E +3	newton (N)
kip/inch^2 (ksi)	6.894 757 x E +3	kilo pascal (kPa)
ktap	1.000 000 x E +2	newton-second/m^2 ($N-s/m^2$)
micron	1.000 000 x E -6	meter (m)
mil	2.540 000 x E -5	meter (m)
mile (international)	1.609 344 x E +3	meter (m)
ounce	2.834 952 x E -2	kilogram (kg)
pound-force (lbs avoirdupois)	4.448 222	newton (N)
pound-force inch	1.129 848 x E -1	newton-meter (N-m)
pound-force/inch	1.751 268 x E +2	newton/meter (N/m)
pound-force/foot^2	4.788 026 x E -2	kilo pascal (kPa)
pound-force/inch^2 (psi)	6.894 757	kilo pascal (kPa)
pound-mass (lbm avoirdupois)	4.535 924 x E -1	kilogram (kg)
pound-mass-foot^2 (moment of inertia)	4.214 011 x E -2	kilogram-meter^2 ($kg-m^2$)
pound-mass/foot^3	1.601 846 x E +1	kilogram-meter^3 (kg/m^3)
rad (radiation dose absorbed)	1.000 000 x E -2	**Gray (Gy)
roentgen	2.579 760 x E -4	coulomb/kilogram (C/kg)
shake	1.000 000 x E -8	second (s)
slug	1.459 390 x E +1	kilogram (kg)
torr (mm Hg, 0^0 C)	1.333 22 x E -1	kilo pascal (kPa)

*The bacquerel (Bq) is the SI unit of radioactivity; 1 Bq = 1 event/s.

**The Gray (GY) is the SI unit of absorbed radiation.

TABLE OF CONTENTS

CONVERSION TABLE iii
LIST OF FIGURES v
PREFACE vi
SUMMARY vii
1.0 INTRODUCTION 1
1.1 MOTIVATION 1
2.0 APPROACH 3
2.1 INHALABILITY MODELING 3
2.2 MODELS OF URT FILTERING EFFICIENCY BY IMPACTION AND BROWNIAN DIFFUSION 5
2.3 LUNG GEOMETRY 8
2.4 LUNG VENTILATION AND PHYSIOLOGY PARAMETERS 8
2.5 MECHANISTIC MODELOF PARTICLE DEPOSITION IN THE LUNG 9
2.6 SOFTWARE IMPLEMENTATION 9
3.0 MODEL PREDICTIONS 11
4.0 CONCLUSIONS 15
5.0 REFERENCES 17
6.0 DEFINITIONS, ACRONYMS, AND ABBREVIATIONS 19

LIST OF FIGURES

Figure 2-1. Compartmental representation of the lung geometry. 6

Figure 3-1. Particle deposition in the lungs of mice via endotracheal breathing. 11

Figure 3-2. Deposition fraction of various size particles at different lung depths. 12

Figure 3-3. Particle deposition in the lungs of B6C3F1 and BALB/c mice via nasal breathing. 13

PREFACE

The research work described in this report was conducted for the Defense Threat Reduction Agency (DTRA) under contract number DTRA01-03-D-0014-0030. The Contract Officer's Representative for this effort was Mr. Rick Fry of DTRA's Information Systems Capability Development Office (J9CBI).

SUMMARY

Assessment of the deposited dose in the lung enables linking of exposure concentration with biological responses. Various strains of mice are used in inhalation studies to study toxicological end points. However, little or no information is available on particle deposition in the lungs of mice. Lung deposition models were developed for particle inhalation in the respiratory tract of BALB/c and B6C3F1 mice. The deposition model included particle inhalability and nasal losses. Particle inhalability in mice was lower than that in rats. In contrast, deposition of the same size particle was higher in mice nasal passages than that in rats. Thus, fewer particles entered the mouse lung in comparison with rat particle inhalation. The penetration was severely limited for micrometer and larger particle sizes. Therefore, relevant and not identical particle sizes to human exposure scenarios must be used for interspecies data extrapolation. Size relevancy issues are addressed by considering compatible deposition of particles in mice and humans.

1.0 INTRODUCTION

The use of various strains of mice in toxicology studies has been on the rise in recent years (e.g., [1–5]) due to the relatively low cost of breeding and husbandry compared with other species, short life cycle to observe long-term health effects, and appropriateness of mice as the surrogate model for certain human biological end points. Under a federally funded research project by the National Institutes of Health, deposition models were developed for two strains of mice (B6C3F1 and BALB/c). These models were included in our multiple-path, particle dosimetry model (MPPD V2.1; Applied Research Associates, Inc., Raleigh, NC) to predict the deposited dose of inhaled biological, chemical, and radiological agents under various exposure scenarios. Coupling of mouse deposition models with those of humans and other species in MPPD allows for dose extrapolation as well as injury and casualty risk analysis for scenarios under which measurements are available in one species but not the others. The deposition model was based on detailed mechanics of airflow and particle transport in the nasal passages and lung airways. The small geometric dimensions of the nostril and low minute ventilation limited the penetration of airborne particles into the respiratory tract of mice. Thus, models of particle inhalability for mice were also developed and integrated into MPPD. Model details and implementation in MPPD are described below.

1.1 MOTIVATION

Injury and casualties resulting from inhalation of an agent are directly related to the deposited dose in the nasal or lung airways. In mice, inter-strain variability in the respiratory tract geometry, breathing parameters, and innate sensitivity warrant strain-specific investigation into deposition and ensuing biological outcome. The availability of measurements of the deposited dose in the lungs of mice is limited. In addition, experiments are expensive and time-consuming, and cannot cover all exposure scenarios. Alternatively, as for other species, mechanistic models can be developed to assess internal dose in mice for various exposure and breathing scenarios. Dosimetry models provide an inexpensive, quick, and efficient means to evaluate the injury or casualty risk associated with inhaled exposure to an agent.

Mechanistically-based particle deposition models were developed to describe the transport and deposition of inhaled particles in the lungs of two strains of mice (B6C3F1 and BALB/c). The deposition models were based on the multiple-path geometry that was previously developed for humans, rats, and rhesus monkeys [6], [7]. Inputs to the model included lung geometry and volumes, and physiological parameters of mice. In addition, models for inhalability and nasal deposition of particles were developed based on information for rats and included in MPPD for mice.

THIS PAGE IS INTENTIONALLY LEFT BLANK.

2.0 APPROACH

The geometry of the respiratory tract is fairly complex. It is made up of thousands of multi-scaled airways with poorly defined shape. In addition, there is a lack of information on airway dimensions for the entire respiratory tract, which includes the tracheobronchial and pulmonary regions. Furthermore, airflow and particle transport through the respiratory system is not quite fully understood. Thus, detailed modeling of particle transport in the entire respiratory system is not possible with the given limited information. However, there have been simplifications for various aspects of the respiratory tract geometry and airflow and particle transport based on observations and experimentations. These simplifications have been incorporated into the deposition model. Consequently, development of a respiratory tract deposition model is divided into several steps, which describe the holistic process of particle transport through lung airways from which the deposited dose of inhaled particles can be computed. The steps describe the derivations of models for particle inhalability and upper respiratory tract (URT) deposition of particles, creation of mice-specific lung geometries and ventilation, and finally, mathematical formulations for particle penetration and deposition through lung airways. While some steps are species-invariant such as ventilation, others are not (e.g., inhalability and URT deposition calculations). Details of each step are presented in the following sections.

2.1 INHALABILITY MODELING

As the particle size becomes larger, its increasing inertia begins to hamper its ability to follow the inhaled airflow streamlines. If the particle deviates significantly from the airflow streamlines, it may fail to enter the URT through the nostrils. Considering a suspension of airborne particles being inhaled into the respiratory tract, the ability of particles to enter the URT, or their inhalability, decreases with increasing particle size. Therefore, models for particle inhalability must be developed to correct for the reduction of exposure concentration due to escaping particles. Particle inhalability is lower in mice than larger size rodents because of the smaller nasal openings of mice. Particles of inhalable sizes in rats and larger rodents may not necessarily be inhalable by mice. Thus, the characterization of particle inhalability is more significant for mice than other rodents.

Semi-empirical relationships have been constructed for particle inhalability as a function of particle inertia based on either laboratory measurements of particle penetration through the URT or computational fluid dynamics analysis, which solves the airflow field and particle transport in the neighborhood of the URT during inhalation. However, no such studies have so far been conducted in mice and a major data gap exists which prevents direct development of particle inhalability models in mice. Considering that mice and rats have similar nasal structures, differing primarily in size and breathing rates, one can perform dimensional analysis to derive equivalent inhalability expressions in mice from existing models in rats. While particle inhalability is related to particle inertia, a literature review reveals that, with the exception of one study [8], particle inhalability has exclusively been related to its diameter. Hence, the effect of breathing rates (and hence inertia) was not accounted for in these studies. Inhalability models that depend on particle diameter alone provide first-order approximation and are not used here.

We adopted the inhalability model of Asgharian et al. [8] for Long-Evans rats and extended it to mice based on dynamic similarities between rats and mice.

Asgharian et al. [8] conducted a series of short-term nose-only inhalation exposure studies in which Long-Evans rats were exposed to monodisperse aerosols ranging in diameter from 0.9 μm to 4.2 μm. Undisturbed aerosol concentration measurements in the exposure environment and measurement-based calculations of URT and LRT deposition fractions were subsequently used to construct a semi-empirical relationship for particle inhalability, or inhalable fraction (IF), in rats as a function of the product of particle aerodynamic diameter (d_{ae}) squared and inhalation flow rate (Q).

$$IF = 1 - \frac{1}{1 + \alpha\left(d_{ae}^2 Q\big|_{Rats}\right)^{\beta}} \tag{1}$$

where $d_{ae}^2 Q$ is the Stokes parameter and is given in $g \times \mu m^2 / s$ with d_{ae} and Q denoting the aerodynamic diameter and inhalation flow rate, respectively. Coefficients α=19.87 and β= -0.7466 were found by fitting equation (1) to the calculated inhalability values [8]. It is assumed that equation (1) equally applies to mice as well, because rats and mice have similar facial and URT geometries, that is inhalability equations in rats and mice are related to the impaction parameter (Stokes number, Stk) by the same relationship. Thus,

$$Stk = \frac{d_{ae}^2 Q}{18\mu D_h}\bigg|_{Rats} = \frac{d_{ae}^2 Q}{18\mu D_h}\bigg|_{Mice} \tag{2}$$

in which μ is the absolute viscosity of air and D_h is the hydraulic diameter of the URT. Hydraulic diameter is defined with respect to the nasal openings in each species because the Stokes number indicates the inertial strength of particles to enter or bypass the nasal opening. By simplifying and rearranging equation (2), the following results are obtained.

$$d_{ae}^2 Q\big|_{Rat} = \frac{D_{h-Rat}}{D_{h-Mouse}} \times d_{ae}^2 Q\big|_{Mouse}, \tag{3}$$

which can be substituted in equation (1) to find

$$IF = 1 - \frac{1}{1 + \alpha\left(\frac{D_{h-Rat}}{D_{h-Mouse}}\right)^{\beta}\left(d_{ae}^2 Q\big|_{Mouse}\right)^{\beta}} \tag{4}$$

where $D_{h-Rat} = 1.065\,mm$ and $D_{h-Mouse} = 0.42\,mm$ are hydraulic diameters for the rat and mouse nasal openings, respectively. Equation (4) is further simplified by substituting for hydraulic diameters.

$$IF = 1 - \frac{1}{1 + \alpha'\left(d_{ae}^2 Q\big|_{Mouse}\right)^{\beta}} \quad (5)$$

Where $\alpha' = 9.92$. Inspection of equation (5) reveals that inhalability in mice is lower than that in rats for the same Stokes parameter. When inhalability predictions in mice and rats are compared, there is an additional reduction of inhalability in mice due to reduced minute ventilation and, hence, a lower Stokes parameter.

2.2 MODELS OF URT FILTERING EFFICIENCY BY IMPACTION AND BROWNIAN DIFFUSION

Deposition of particles in the mouse URT occurs by two distinct mechanisms. For sub-micrometer and smaller particles, Brownian diffusion is responsible for the removal of particles from the inhaled air. In contrast, inertial impaction is the dominant mechanism of deposition of particles in the nasal passages for sub-micrometer and larger particle sizes. Particle deposition by sedimentation is negligible in the mouse URT due to the small residence time of particles in the airway passages.

Approaches for calculating particle deposition in the URT of mice are similar to those proposed for inhalability assessment, which are either based on experimental measurements or computational fluid dynamics analysis. In this case, neither approach is feasible due to the lack of information. Therefore, the models developed in other rodents with similar URT geometry to mice will be extended to mice by making proper adjustments.

There are no computational fluid dynamics studies available for deposition of sub-micrometer and larger particles sizes in the URT of mice. However, particle deposition has been measured in the URT and LRT of CD1 mice [9]. Raabe et al. [9] conducted a nose-only exposure, in which CD1 mice were exposed briefly to monodisperse aerosols ranging in size from 0.27 μm to 9.65 μm. The exposure was composed of mainly fine and coarse particles. Hence, the reported measurements reflected deposition primarily by inertial impaction and included deposited masses of particles in the nasal and lung airways. Exposure atmosphere was also sampled at an available exposure port of the nose-only exposure unit. These measurements were used here to calculate regional deposition fraction of particles by dividing the deposited mass in a given region by the mass of inhaled particles during the inhalation study. In a simple-minded scenario, one may assume the respiratory tract is represented by URT and LRT compartments while breathing is approximated to be steady-state, justifiable by the fact that the Womersley number (ratio of inertial to viscous forces - a measure of flow unsteadiness) is very small. It may further be assumed with reasonable accuracy that URT deposition efficiencies during inhalation and exhalation are similar. Referring to Figure 2-1, deposition fractions in the head and lung are found from the following relationships:

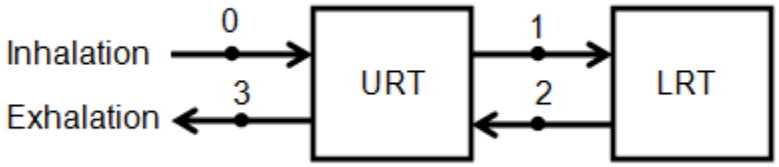

Figure 2-1. Compartmental representation of the lung geometry.

$$m_{URT} = m_{in} \times \eta_{URT-imp} + (m_{in} - m_{in} \times \eta_{URT-imp} - m_{LRT}) \times \eta_{URT-imp} \quad (6)$$

in which $\eta_{URT-imp}$ is the deposition efficiency of particles in the URT by impaction during inhalation and exhalation, m_{in} is the mass of inhaled particles, and m_{URT} and m_{LRT} are masses of particles deposited in the URT and LRT, respectively. Dividing both sides of equation (6) by m_{in} and solving for η_{URT} gives

$$\eta_{URT-imp} = \left(1 - \frac{\Delta_{LRT}}{2}\right) - \sqrt{\left(1 - \frac{\Delta_{LRT}}{2}\right)^2 - \Delta_{URT}} \quad (7)$$

In which $\Delta_{URT} = m_{URT} / m_{in}$ and $\Delta_{LRT} = m_{LRT} / m_{in}$ are deposition fractions of particles in the URT and LRT. Measured mass of deposited particles in the URT and LRT from the experiment of Raabe et al. [9] were used to calculated regional deposition fractions and URT deposition efficiency (equation (7)) for each particle size used in the experiment. Calculated URT efficiencies were fit to a logistic function suggested by Zhang and Yu [10] to obtain an expression for particle deposition by impaction in the URT of mice.

$$\eta_{H-imp} = \left[\frac{(d_{ae}^2 Q)^{\alpha}}{10^5 + (d_{ae}^2 Q)^{\alpha}}\right]^{\beta} \quad (8)$$

Since animals' minute ventilations were not reported by Raabe et al. [9], the empirically-derived equation of Guyton [11] was used in equation (8) to find $\alpha = 3.96$ and $\beta = 0.117$ with $R^2 = 0.98$.

There is no information on deposition of ultrafine particles in the URT of mice either by measurements or theoretical modeling. Comparison of the nasal structure of mice with the same for rats reveals similar dominant features while exhibiting typical fine intra- and inter-subject variations. Thus, for predictions with order-of-magnitude level of accuracy, the nasal geometries of the two species are assumed to be similar, which allows deposition models for ultrafine particles in rats to be extended to mice. Based on measurements in the nasal casts of rats, Cheng et al. [12] obtained the following expression for losses of ultrafine particles in the nasal passages of rats by Brownian diffusion during inhalation and exhalation.

$$\eta_{URT-diff} = 1 - e^{-\alpha D^{\beta} Q^{\gamma}} \quad (9)$$

where D is the particle diffusion coefficient (cm^2/sec) and Q is the inhalation or exhalation flow rate (L/min). Coefficients α, β, and γ were found by curve fitting the measurements to equation (9) [12]. While deposition efficiency by Brownian diffusion in equation (9) is explicitly described in terms of the diffusion coefficient and breathing flow rate, the more general form of the equation, which will include inter-subject variability, is given by

$$\eta_d = 1 - e^{-\alpha' Sc^{\beta'} Pe^{\gamma'}} \tag{10}$$

where Schmidt number (Sc) and Peclet (Pe) numbers are given by

$$\begin{cases} Sc = \dfrac{\nu}{D} \\ Pe = \dfrac{4Q}{\pi D D_h} \end{cases} \tag{11}$$

In which ν is the kinematic viscosity of air. Substituting for Sc and Pe in equation (10) and rearranging variables gives

$$\eta_d = 1 - e^{-\alpha' \nu^{\beta'} \left(\frac{4}{\pi}\right)^{\gamma'} D_h^{-\gamma'} D^{-(\beta'+\gamma')} Q^{\gamma'}} \tag{12}$$

Because of geometric similarity of nasal passages, equation (12) denotes deposition efficiency by diffusion in the nasal passages of both rats and mice. Equating the exponential term of equation (12) for the case of the two species gives

$$D_{Rats}^{-(\beta'+\gamma')} Q_{Rats}^{\gamma'} = \left(\frac{D_{h_{Rats}}}{D_{h_{Mice}}}\right)^{\gamma'} D_{Mice}^{-(\beta'+\gamma')} Q_{Mice}^{\gamma'} \tag{13}$$

By letting $\beta = -(\beta'+\gamma')$ and $\gamma = \gamma'$, it becomes apparent that deposition efficiency by diffusion in the URT of mice can be described by

$$\eta_d = 1 - e^{-\alpha \left(\frac{D_{h-Rats}}{D_{h-Mice}}\right)^{\gamma} D_{Mice}^{\beta} Q_{Mice}^{\gamma}} \tag{14}$$

Hence equation (9) can be used to calculate URT losses in mice simply by scaling the coefficient α by $(D_{h-Rats} / D_{h-mice})^{\gamma}$. It is noted that hydraulic diameters in equation (14) are defined based on volume and surface area of the nasal passages whereas those in equation (4) are based on the perimeter and cross-sectional area of the nostril. Replacing for the values of hydraulic diameters in rats and mice it is found that α = 13.688 and 11.407 for inhalation and exhalation, respectively, while β = 0.517 and γ = -0.234 remain the same as for rats.

2.3 LUNG GEOMETRY

Measurements of lung airway parameters such as length, diameter, gravity and bifurcation angles are difficult to make due to the enormous number of airways and complexity of airway shape and lung structure. Measurements are typically made along selected pathways spanning from the trachea down to terminal bronchioles for the conducting airways. The same measurements are made for the pulmonary airways including respiratory bronchioles, alveolar ducts, and alveolar sacs in the selected paths and are complemented by measuring the size of the alveoli and the number of alveoli per duct. Modeling each airway as a cylindrical tube and the lung as a branching network of airways, representative, typical-path, dichotomous and asymmetric lung geometries have been constructed for a variety of species.

14-generation, typical-path, symmetric tracheobronchial airway geometries for two strains of mice (B6C3F1 and BALB/c) were constructed. The method proposed by Oldham et al. [13] was followed to incorporate the monopodial lung structure for the tracheobronchial region. Instead of doubling in number which is common with symmetric dichotomous lung geometries, the number of airways per generation increased by 1.5^n for a linear increase between generation 5 (trachea being considered as generation 0) and the terminal bronchioles (1505 and 1584 for B6C3F1 and BALB/c mice, respectively). Airway lengths and diameters were also rescaled to lung total capacity for consistency with other lung geometry databases in MPPD. Reported airway measurements of Oldham et al. [13] and Phalen [14] were used for the B6C3F1 lung geometry. The lung geometry of BALB/c mouse was from the measurements of Oldham and Phalen [13] and Oldham and Robinson [15].

For the pulmonary region, Oldham and Robinson [15] for the BALB/c mouse and Oldham et al. [13] and Phalen [14] for the B6C3F1 mouse proposed an 8-generation, typical-path dichotomous branching alveolar geometry. The alveolar branching structure was attached to the distal end of the terminal bronchioles in the tracheobronchial tree to complete the lung structure for BALB/c and B6C3F1 mice.

It is worth noting that airway parameters had to be rescaled twice prior to deposition calculations in each strain of mouse: first by $(\mathrm{FRC}/\mathrm{TLC})^{1/3}$, where FRC is the functional residual capacity or lung volume at rest and TLC is the total lung capacity, to adjust airway dimensions to rest conditions, and second by $(1+\mathrm{V_T}/2)^{1/3}$, where $\mathrm{V_T}$ is the tidal volume, to account for airway size change during breathing. The rescaled lung geometry was used in the calculations of particle deposition in the lung.

2.4 LUNG VENTILATION AND PHYSIOLOGY PARAMETERS

Lung ventilation is driven by the difference in pressure between the pleural space and the outside environment. The pressure drop due to the lung compliance and airway resistance will produce airflow in lung airways during inhalation and exhalation. In principle, airflow through an airway is determined from the solution of the mass and momentum balance equations for the entire lung geometry. Airflow distribution in different lobes and airways of the lung is directly related to lung expansion and contraction rates and influenced by the gravity-induced intra-pleural pressure

variation. However, lung expansion and contraction is uniform in rodents because rodents are typically positioned horizontally. The airflow rate entering each daughter airway of an airway bifurcation under such circumstances is shown for uniform lung expansion and contraction to be proportional to the distal volume to each daughter airway branch [16]. Hence, airflow rate through all lung airways is calculated by traversing down the lung tree and calculating flow rates in daughter branches of an airway bifurcation from the parent airflow rate and distal-volume proportionality of daughter branches.

Various physiological parameters such as V_T, TLC, FRC, and URT volume were needed to calculate inhalation and exhalation flow rates at the trachea from which flow rates in subsequent airways could be determined. The measured physiological parameters from the double chamber plethysmograph study of DeLorme and Moss [17] were used to determine default breathing frequency, inhalation and exhalation breathing fractions, and V_T for BALB/c and B6C3F1 mice. The TLC was calculated by summing up the individual airway volumes and alveolar volumes for the BALB/c and B6C3F1 lung geometries. FRC and URT volume were determined by extrapolating from proportional ratios in rats (FRC/TLC ~ 30% and URT/TLC ~ 3%).

2.5 MECHANISTIC MODELOF PARTICLE DEPOSITION IN THE LUNG

The particle mass conservation or convective-diffusion equation was developed by accounting for the number of particles that entered, exited, deposited and remained suspended in an airway per unit time [18–20]. It was assumed that particle concentration was uniform across the airway cross section but varied with time and location within the airway. First, particle concentration reaching the trachea was calculated by including the filtering effects of the URT by Brownian diffusion and inertial impaction. Next, the convective-diffusion equation was solved in the lung geometry of B6C3F1 or BALB/c mouse one airway at a time starting from the trachea and traversing down the lung tree to find particle concentration throughout the lung during inhalation, pause, and exhalation. Particles were carried through lung airways by the airflow generated by a uniform expansion and contraction of lung lobes as described in the previous section. Finally, particle deposition in each airway of the lung was calculated by integrating particle flux over time and airway volume. Deposition fraction of inhaled particles per airway, lobe, and region of the lung was found by dividing the calculated deposition by the mass of inhaled particles. Particle deposition fraction is a unique property for a given lung geometry and breathing parameters. Local or regional mass deposited or number of particles deposited was calculated by multiplying the deposition fraction by the mass or number of particles inhaled, respectively.

2.6 SOFTWARE IMPLEMENTATION

We modified the existing MPPD software application to incorporate the B6C3F1 and BALB/c mouse respiratory deposition models described above. First, the particle inhalability, nasal diffusion efficiency, and nasal impaction efficiency equations were implemented in the MPPD code. Next, we created geometry data files used to represent the trachebronchial and pulmonary airway structure in both strains of mouse. The files contained airway length, diameter, branching and gravity angle, and alveolar volume (for pulmonary airways) information for each airway generation. The geometry data files were used as input by MPPD to form the tree branching

structure within which particle transport and deposition were calculated. Slight modifications to the code were necessary to accommodate the monopodial (instead of the typical dichotomous branching structure) nature of the mouse respiratory tract. Default respiratory tract volume and breathing parameters were determined for the mouse model based on available measurements [17], [21]. Particle transport and deposition within the mouse lung airways was calculated in the same manner as other animal models and implemented as described in the preceding section.

The MPPD graphical user interface (GUI) was modified to accommodate the addition of the two new mouse models. The B6C3F1 and BALB/c strains are now among the options in the input dialog for animal geometry. Once either mouse model is chosen, realistic mouse respiratory tract volumes (URT, FRC, TLC) and breathing parameters (V_T, breathing frequency, and inspiratory/expiratory fraction) are selected as default starting values for the deposition model. These values may be changed at the user's discretion. Once these values are entered and the inhaled aerosol characteristics are defined by the user, the model may be executed. Deposition predictions are generated by region (URT, TB, pulmonary, LRT) and also by generation number. Text reports containing a summary of the model predictions and tabulated deposition totals as well as graphical plots of deposition predictions may be generated by the user. These time-stamped reports and plots also contain logs of the input values used for the predictions and may be saved and/or printed for future reference.

3.0 MODEL PREDICTIONS

Regional deposition in the LRT was calculated for B6C3F1 and BALB/c strains of mice for which lung geometry and physiological parameters are described above. To study the influence of lung geometry alone on particle deposition, the same physiological parameters were used in the computations, which included a URT volume of $0.0315\,cm^3$ [21], lung FRC of $0.3\,cm^3$ [17], V_T of $0.2\,cm^3$ [17], average breathing frequency of 300 breaths/min, and 0.4 for inspiratory fraction with no pause between inhalation and exhalation [17].

Particle deposition in the mouse lungs is suspected to vary by strain. To study the influence of lung geometry on particle deposition, particle deposition fractions in the lungs of B6C3F1 and BALB/c mice were calculated via endotracheal breathing (i.e., no head losses) for the same lung and breathing parameters stated above. Predicted deposition fractions are given in Figure 3-1 for the tracheobronchial (TB) and pulmonary (PUL) regions and the sum (LRT) of deposition fractions in the two regions. The shapes of the regional deposition fraction curves were similar in the two strains. Particle deposition was greater in the BALB/c mouse lung than that in B6C3F1 mouse. TB deposition was only slightly different and nearly identical for 0.1 μm and greater size particles. For ultrafine particles, the difference in TB deposition increased with decreasing particle size but did not exceed 4%. There was a greater inter-strain difference in deposition fraction in the pulmonary region. The largest difference was found to be about 8% for 0.03-μm and 10-μm particle sizes in the pulmonary region. Overall, there was a maximum 9% deposition difference in the LRT region, which occurred for 0.02 μm size particles. Thus, adjustments are necessary to correct for strain-specific particle deposition in the mice lungs.

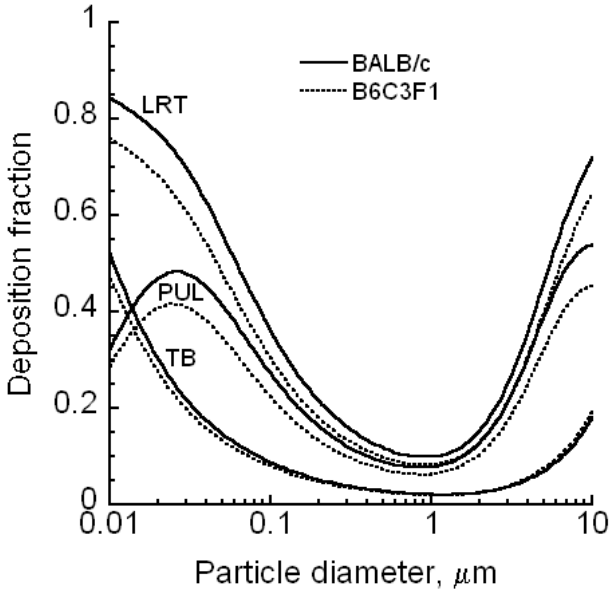

Figure 3-1. Particle deposition in the lungs of mice via endotracheal breathing.

The calculated deposition fractions of particles in the lung are plotted against generation number in Figure 3-2 for the case of nasal breathing to examine deposition distribution throughout the LRT. Deposition fraction decreased for both strains of mice with increasing particle size partly due to aerodynamic properties and partly due to the reduction in respirability with increasing particle size. Deposition of 1-μm particles was negligible in the TB region and peaked in distal generations of the LRT. Deposition fractions of 0.01- and 0.1-μm particles increased with lung depth (generation number) until airborne particles were depleted from the inhaled air after which deposition fraction dropped to zero. The results indicated that to reach the deepest regions of the lung with significant deposition, particle size should have been around 0.1 μm . Smaller size particles had a higher upper airway deposition. Larger particles demonstrate reduced respirability which prevented them from reaching the deep lung. It is interesting to note that no significant impaction deposition occurred in the first few upper airways of the lung because particle sizes were smaller than 1 μm . The results also confirmed that for the same physiological parameters, particle deposition was higher in BALB/c mice than in B6C3F1 mice. The difference was most notable in the alveolar region, which has the greatest deposition fractions.

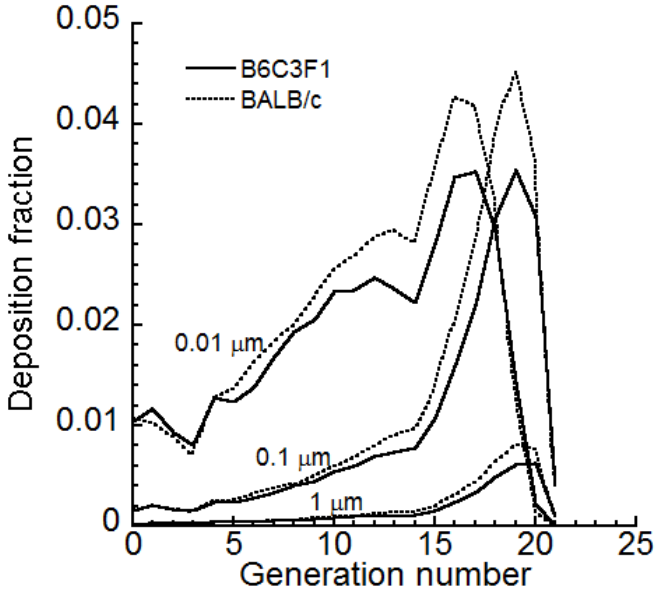

Figure 3-2. Deposition fraction of various size particles at different lung depths.

Regional deposition fractions of particle with sizes between 0.01 and 10 μm in the respiratory tracts of both mouse strains are given in Figure 3-3 via nasal breathing for the same physiological parameters stated above. Comparison of predicted deposition fractions in the LRT region via nasal breathing with those for the case of endotracheal breathing (Figure 3-1) showed similar patterns for submicrometer-sized particles but drastic differences for fine and coarse particles. The differences were caused by the effects of particle inhalability and nasal deposition which severely reduced the number of particles that reached the LRT. There was a slight reduction in inhalability and some deposition in the nasal passages for ultrafine particles. As a result, the regional deposition curves via nasal breathing decreased modestly compared with those for endotracheal breathing. Impaction losses increased substantially for fine and coarse

particles to reach 100% for 2 μm particles beyond which there was no penetration of particles into the LRT. Consequently, the regional deposition curves for nasal breathing dropped significantly.

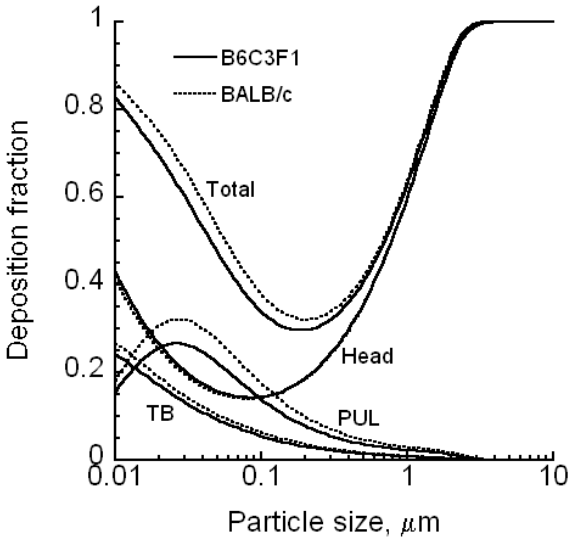

Figure 3-3. Particle deposition in the lungs of B6C3F1 and BALB/c mice via nasal breathing.

THIS PAGE IS INTENTIONALLY LEFT BLANK.

4.0 CONCLUSIONS

A particle deposition model was developed for the lungs of BALB/c and B6C3F1 mice and used to predict losses of particles inhalable to humans. Model predictions showed that only submicrometer particles can penetrate and deposit in the lungs of mice. Ultra fine particle deposition fraction was more significant in the pulmonary region than in the TB region. There was a significant deposition of large particles in the nasal passages of mice. The deposition fraction of 1 μm or larger particles was only about a few percent. Particles larger than 2 μm were not capable of penetrating past the mouse nasal passages. Comparison of model predictions for the two strains of mice showed that while the deposition patterns were similar, there were differences in the predicted deposition fraction. Thus, strain-specific deposition models should be developed for mice to study the dose and biological end points.

THIS PAGE IS INTENTIONALLY LEFT BLANK.

5.0 REFERENCES

[1] J. K. Dunnick, M. R. Elwell, J. M. Benson, C. H. Hobbs, F. F. Hahn, P. J. Haly, Y. S. Cheng, and A. F. Eidson, "Lung toxicity after 13-week inhalation exposure to nickel oxide, nickel subsulfide, or nickel sulfate hexahydrate in F344/N rats and B6C3F1 mice," *Fundam Appl Toxicol*, vol. 12, no. 3, pp. 584–594, Apr. 1989.

[2] Z. Korsak, W. Majcherek, and K. Rydzyński, "Toxic effects of acute inhalation exposure to 1-methylnaphthalene and 2-methylnaphthalene in experimental animals," *Int J Occup Med Environ Health*, vol. 11, no. 4, pp. 335–342, 1998.

[3] J. M. Benson, R. L. Carpenter, F. F. Hahn, P. J. Haley, R. L. Hanson, C. H. Hobbs, J. A. Pickrell, and J. K. Dunnick, "Comparative inhalation toxicity of nickel subsulfide to F344/N rats and B6C3F1 mice exposed for 12 days," *Fundam Appl Toxicol*, vol. 9, no. 2, pp. 251–265, Aug. 1987.

[4] J. M. Benson, I.-Y. Chang, Y. S. Cheng, F. F. Hahn, E. B. Barr, K. R. Maples, and M. B. Snipes, "Species differences in the fate of nickel compounds in the respiratory tract," Inhalation Toxicology Research Institute (ITRI), Lovelace Biomedical and Environmental Research Institute, Albuquerque, NM, Final report NiPERA, 1995.

[5] National Toxicology Program (NTP), "Toxicology and carcinogenesis studies of vanadium pentoxide (Case 1314-62-1) in F-344/N rats and B6C3F1 mice (inhalation studies)," U.S. Department of Health and Human Services, Public Health Service, National Insitutes of Health, Research Triangle Park, NC, NTP Technical Report Number 507, NIH Publication Number 03-4441, 2002.

[6] O. T. Price, B. Asgharian, F. J. Miller, F. R. Cassee, and R. de Winter-Sorkina, "Multiple Path Particle Dosimetry Model (MPPD v1.0): A model for human and rat airway particle dosimetry," National Institute for Public Health and the Environment (RIVM) Report 650010030, 2002.

[7] B. Asgharian, O. T. Price, G. E. McClellan, R. Corley, D. R. Einstein, R. E. Jacob, J. R. Harkema, S. A. Carey, E. Schelegle, D. Hyde, J. S. Kimbell, and F. J. Miller, "Development of a rhesus monkey lung geometry model and application to particle deposition in comparison to humans," *Inhalation Toxicology,* vol. 24, no. 3, pp. 182-193.

[8] B. Asgharian, J. T. Kelly, and E. W. Tewksbury, "Respiratory Deposition and Inhalability of Monodisperse Aerosols in Long-Evans Rats," *Toxicol Sci*, vol. 71, no. 1, pp. 104 –111, Jan. 2003.

[9] O. G. Raabe, M. A. Al-Bayati, S. V. Teague, and A. Rasolt, "Regional deposition of inhaled monodisperse coarse and fine aerosol particles in small laboratory animals," *Ann Occup Hyg*, vol. 32 (inhaled particles VI), pp. 53–63, 1988.

[10] L. Zhang and C. P. Yu, “Empirical Equations for Nasal Deposition of Inhaled Particles in Small Laboratory Animals and Humans,” *Aerosol Sci Tech*, vol. 19, no. 1, pp. 51–56, 1993.

[11] A. C. Guyton, “Measurement of the respiratory volumes of laboratory animals,” *Am J Physiol*, vol. 150, no. 1, pp. 70–77, Jul. 1947.

[12] Y. S. Cheng, G. K. Hansen, Y. F. Su, H. C. Yeh, and K. T. Morgan, “Deposition of ultrafine aerosols in rat nasal molds,” *Toxicol Appl Pharmacol*, vol. 106, no. 2, pp. 222–233, Nov. 1990.

[13] M. J. Oldham, R. F. Phalen, G. M. Schum, and D. S. Daniels, “Predicted nasal and tracheobronchial particle deposition efficiencies for the mouse,” *Ann Occup Hyg*, vol. 38, no. inhaled particles VII, pp. 135–141, 1994.

[14] R. F. Phalen, “An airway model for the laboratory mouse,” NiPERA, Nov. 1991.

[15] M. J. Oldham and R. J. Robinson, “Predicted tracheobronchial and pulmonary deposition in a murine asthma model,” *Anat Rec (Hoboken)*, vol. 290, no. 10, pp. 1309–1314, Oct. 2007.

[16] C. P. Yu, “Exact analysis of aerosol deposition during steady breathing,” *Powder Technol*, vol. 21, no. 1, pp. 55–62, Sep. 1978.

[17] M. P. DeLorme and O. R. Moss, “Pulmonary function assessment by whole-body plethysmography in restrained versus unrestrained mice,” *J Pharmacol Toxicol Methods*, vol. 47, no. 1, pp. 1–10, Feb. 2002.

[18] S. Anjilvel and B. Asgharian, “A multiple-path model of particle deposition in the rat lung,” *Fundam Appl Toxicol*, vol. 28, no. 1, pp. 41–50, Nov. 1995.

[19] B. Asgharian, W. Hofmann, and R. Bergmann, “Particle Deposition in a Multiple-Path Model of the Human Lung,” *Aerosol Sci Tech*, vol. 34, no. 4, pp. 332–339, 2001.

[20] B. Asgharian and O. T. Price, “Deposition of ultrafine (nano) particles in the human lung,” *Inhal Toxicol*, vol. 19, no. 13, pp. 1045–1054, Oct. 2007.

[21] L. B. Méndez, G. Gookin, and R. F. Phalen, “Inhaled aerosol particle dosimetry in mice: a review,” *Inhal Toxicol*, vol. 22 Suppl 2, pp. 15–20, Dec. 2010.

6.0 DEFINITIONS, ACRONYMS, AND ABBREVIATIONS

ARA	Applied Research Associates, Inc
B6C3F1	Designation for a specific laboratory mouse strain
BALB/c	Designation for a specific laboratory mouse strain
CD1	Designation for a specific laboratory mouse strain
DTRA	Defense Threat Reduction Agency
FRC	Functional Residual Capacity
LRT	Lower Respiratory Tract
μm	Micrometer or micron, see Conversion Table
MPPD	Multiple-Path Particle Dosimetry Model
PUL	Pulmonary
Q	Flow rate
TB	Tracheobronchial
TLC	Total Lung Capacity
URT	Upper Respiratory Tract

DISTRIBUTION LIST
DTRA-TR-15-16

DEPARTMENT OF DEFENSE

DEFENSE TECHNICAL INFORMATION CENTER
8725 JOHN J. KINGMAN ROAD, SUITE 0944
FT. BELVOIR, VA 22060-6218
ATTN: DTIC

QUANTERION SOLUTIONS, INC.
1680 TEXAS STREET, SE
KIRTLAND AFB, NM 87117-5669
ATTN: DTRIAC

JOINT PROJECT MANAGER INFORMATION SYSTEMS (JPM IS)
JOINT PROGRAM EXECUTIVE OFFICE FOR
CHEMICAL BIOLOGICAL DEFENSE (JPEO-CBD)
301 PACIFIC HIGHWAY
SAN DIEGO, CA 92110

DEFENSE THREAT REDUCTION AGENCY
8725 JOHN J. KINGMAN ROAD
FT. BELVOIR, VA 22060-6201
ATTN: DR. CHRISTOPHER KILEY /J9CBA

DEFENSE THREAT REDUCTION AGENCY
8725 JOHN J. KINGMAN ROAD
FT. BELVOIR, VA 22060-6201
ATTN: MR. JERRY GLASOW /J9CBI

DEFENSE THREAT REDUCTION AGENCY
8725 JOHN J. KINGMAN ROAD
FT. BELVOIR, VA 22060-6201
ATTN: MR. RICHARD FRY /J9CBI

DEFENSE THREAT REDUCTION AGENCY
8725 JOHN J. KINGMAN ROAD
FT. BELVOIR, VA 22060-6201
ATTN: MR. THOMAS WOLFINGER /J9CBI

DEFENSE THREAT REDUCTION AGENCY
8725 JOHN J. KINGMAN ROAD
FT. BELVOIR, VA 22060-6201
ATTN: DR. ERIN REICHERT /J9CBM

DEFENSE THREAT REDUCTION AGENCY
8725 JOHN J. KINGMAN ROAD
FT. BELVOIR, VA 22060-6201
ATTN: DR. RON MERIS /J9ISR

DEFENSE THREAT REDUCTION AGENCY
8725 JOHN J. KINGMAN ROAD
FT. BELVOIR, VA 22060-6201
ATTN: DR. AIGUO WU /J9ISR

DEPARTMENT OF DEFENSE CONTRACTORS

APPLIED RESEARCH ASSOCIATES, INC
SECURITY ENGINEERING AND APPLIED SCIENCES
119 MONUMENT PLACE
VICKSBURG, MS 39180-5156
ATTN: MR. JOSEPH L. SMITH